CONF-9505264--2

UCRL-JC-121148
PREPRINT

The Measurement and Analysis of Wavefront Structure from Large Aperture ICF Optics

C. R. Wolfe
J. K. Lawson

This paper was prepared for submittal to the
1st Annual Solid-State Lasers for Application
to Inertial Confinement Fusion
Monterey, CA
May 30-June 2, 1995

May 30, 1995

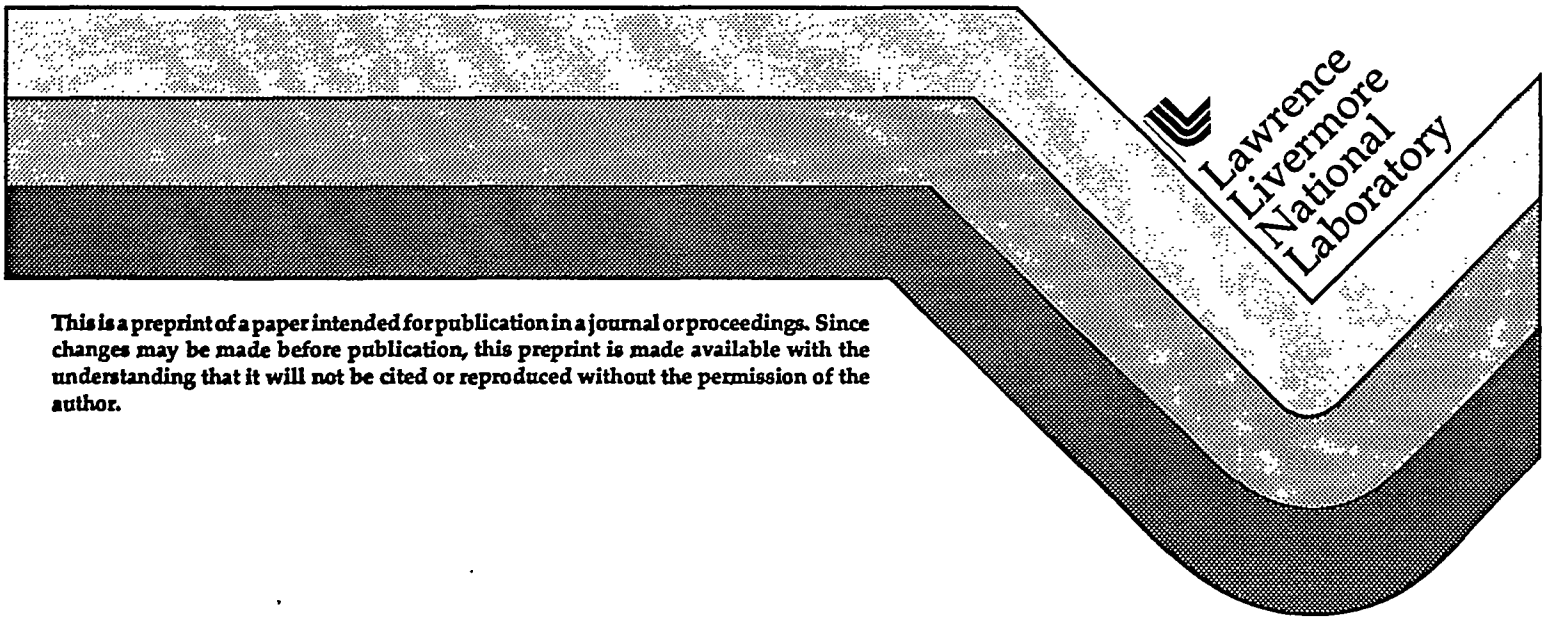

The measurement and analysis of wavefront structure from large aperture ICF optics

C. R. Wolfe, J. K. Lawson

Lawrence Livermore National Laboratory, L-487
P. O. Box 5508 Livermore, Ca., 94550

ABSTRACT

This paper discusses the techniques, developed over the past year, for high spatial resolution measurement and analysis of the transmitted and/or reflected wavefront of large aperture ICF optical components. Parts up to 400 mm x 750 mm have been measured and include: laser slabs, windows, KDP crystals and lenses. The measurements were performed using state-of-the-art commercial phase shifting interferometers at a wavelength of 633 μm. Both 1 and 2-D Fourier analysis have been used to characterize the wavefront; specifically the Power Spectral Density, (PSD), function was calculated. The PSDs of several precision optical components will be shown. The PSD(v) is proportional to the (amplitude) ^{2} of components of the Fourier frequency spectrum. The PSD describes the scattered intensity and direction as a function of scattering angle in the wavefront. The capability of commercial software is limited to 1-D Fourier analysis only. We are developing our own 2-D analysis capability in support of work to revise specifications for NIF optics. 2-D analysis uses the entire wavefront phase map to construct 2-D PSD functions. We have been able to increase the signal-to-noise relative to 1-D and can observe very subtle wavefront structure.

The physics of the NIF laser design dictates partitioning the wavefront into three regimes of spatial wavelength (or spatial frequency). We will discuss the data in terms of the following three scale length regimes:

i. short scale, or "micro roughness", having scale lengths < 120 μm
ii. mid-spatial scale, with scale lengths from 0.12 to 33 mm, and
iii. long scale, or conventional "optical figure/curvature" , having scale lengths > 33 mm.

Regular repetitive wavefront structure has been observed in all three regimes, ranging from 10 μm to 100 mm in scale length. The magnitude of these structures are typically from λ/100 to λ/20 Structure has been detected in optical materials and on the surfaces of finished parts. We believe the sources of these structures are small fabrication errors. The Modeling Group at LLNL is using this data in beam propagation codes, to assist in optimizing laser system design and to develop optics specifications for the NIF.

Keywords: phase measuring interferometry, Power Spectral Desnsity, PSD, wavefront analysis Fourier analysis

1. INTRODUCTION

Future inertial confinement fusion (ICF) lasers systems such as the National Ignition Facility (NIF) will require optical components with clear apertures on the order of 400 mm square. High spatial resolution measurement of the wavefront of parts of this size is now possible due to the highly developed instrumentation and techniques of phase shifting interferometry. The wavefront data that can now be obtained from proto-type parts will help establish the design basis of such lasers. This data will provide:

i. information about wavefront modulation for beam propagation modeling, laser system design and optimization,
ii. metrology data for optical component specification and
iii. a baseline of component wavefronts to assist in the development of advanced fabrication processes.

During the last two decades the analysis capability and the spatial resolution of wavefront measurements for large apertures has greatly increased. Previously, only low resolution cameras were available and were used to detect phase information for scale lengths > 10 mm from static interferograms. This data was processed by fringe centering algorithms which digitized the interferogram and interpolated the location of fringe centers. At best, several hundred data points were calculated. With only low frequency data, the wavefront was often constructed by fitting the data to Zernicke polynomials. This was the state of commercial instrumentation for wavefront analysis in the late '70s [1]. Today, the state of the art has changed greatly. High resolution solid state cameras, advanced phase shifting interferometry techniques and advanced computational algorithms are available to detect and calculate wavefront shape. Wavefront data can be obtained at each pixel of the high resolution solid state detector. Detectors with 640 x 480 or 740 x 480 pixels are common [2] in interferometry applications. Larger "mega-pixel" arrays, while not as common, are also available [3]. Equipped with high resolution detectors, modern interferometers are capable of exceeding 1 mm spatial resolution for test apertures of 400 x 400 mm size. Advanced phase shifting algorithms have, for the most part, replaced fringe centering algorithms. Modern algorithms that calculate the wavefront shape now routinely use data sets containing > 300,000 data points, rather than only points at interpolated fringe centers. Fourier analysis is replacing Zernicke polynomial fits, in many applications, when wavefront reconstruction is performed with high resolution data.

2. WAVEFRONT MEASUREMENT

2.1 Instrument description

The wavefront measurements that are reported here have been made over the last year, using three commercial instruments:

i. a 4" / 12" aperture Zygo Mark IVxp® phase shifting Fizeau interferometer,
ii. a Maxim 3D® interference microscope equipped with Fizeau and Mirau type objectives. Both of these instruments are owned by the Materials & Measurement Engineering Division at LLNL, and
iii. a 4" / 18" aperture Zygo GPIxp® phase shifting Fizeau interferometer, owned by the Laser Program at LLNL

Each of these instruments are mounted on a conventional air suspension tables for isolation from environmental vibrations. The first two instruments are located in general purpose precision metrology laboratories with temperature control of approximately 68 ± 2.5 °F. The third instrument is located in a class 1000 cleanroom designed for fabrication of large aperture diffraction gratings, temperature control of that area is approximately 68 ± 1.0 °F. Optical testing with these instruments is performed only by authorized personnel using approved, documented optical inspection and test procedures. A sketch of the optical layout and photographs of the GPIxp Fizeau interferometer are shown in Figure 1. This instrument will be used extensively for metrology studies of large aperture ICF optical components in the future. It has the following capability:

i. two main test arms of 102 / 457 mm (4" / 18") diameter aperture arranged in parallel, a turn mirror selects aperture to be used,
ii. a third, 33 mm diameter aperture, achieved by using a beam reduction telescope on the 102 mm arm,
iii. continuously variable magnification from 1 - 6x,
iv. a long coherence length, circular polarized light source with wavelength of 633 nm,
v. a solid state camera with 640 x 480 pixels (Sony commercial video),
vi. measurement and data analysis are controlled with MetroPro® Rev. 6.0 software operated by a HP 715 series computer with a UNIX® Rev 9.0 operating system, and
vii. data transfer via "Ethernet" to / from other interferometers and computers used for wavefront analysis.

2.2 Bandwidth

The phase map shown in Figure 2 is a 38 mm square reflected wavefront from a diamond turned KDP crystal. It was measured with a 256 x 256 camera. With an aperture of this size we can observe repetitive features with maximum lengths of approximately 1/3 of the aperture dimension (approximately 13 mm). The shortest scale length that can be observed is approximately 3x the ideal, Nyquist limited resolution. This lower limit is is approximately 0.9 mm. A modulation

with spatial scale of 4 - 6 mm is clearly visible in Figure 2. On the other hand, the diamond tool feed marks, which have a scale length of approximately 4 μm, are not visible. These short scale length (high frequency) features lie outside the bandwidth of the measurement.

The bandwidth is determined by the composite optical transfer function (OTF) of the instrument [4]. For an interferometer with a long coherence length source (the type used here) the transfer function is composed of contributions from the instrument optical system and the camera, or detector. Absolute wavefront characterization requires that the transfer function be measured or calculated accurately, to determine instrument frequency response. The interferometer OTF(ν) can be determined by measuring the wavefronts from known phase objects and calculating the Fourier transform from the data. The OTF(ν) is the ratio of the measured Fourier amplitude spectrum to the ideal Fourier amplitude spectrum of the phase structure:

$$OTF(\nu) = A(\nu)_{measured} / A(\nu)_{calculated} .$$

Raw wavefront data can be corrected or "restored" after the mesurement by accounting for the instrument OTF(ν). This is done by multiplying the Fourier amplitudes, A(ν), in the spectrum, by 1 / OTF(ν) and then taking the inverse transform. The "restored" wavefront will contain increased amplitudes for high frequency features compared to the raw wavefront. We are currently developing the capability to correct data that is used for propagation modeling in this way.

If comparative wavefront measurement is the object of the measurement (as is the case when writing specifications that include the test method, or for process monitoring) raw wavefront data uncorrected for bandwidth effects can be used. Measurements are in process to determine the OTF(ν) for the instruments as mentioned above: the phase maps shown below are raw data.

The spatial bandwidth can be extended by varying the interferometer aperture and/or the detector size (pixel count). This is illustrated in Figure 3, which shows how the "ideal" or detector limited bandwidth varies as interferometer aperture or detector pixel count is varied. In principle, wide bandwidth information can be obtained from multiple aperture measurements to yield data unobtainable from a single measurement. If absolute wavefront data is required, the instrument OTF(ν) must be known at each aperture used.

2.3 Metrology requirements

The performance of high peak power laser systems can be seriously degraded by the presence of low amplitude periodic modulations in the surface and transmitted wavefronts of the optical components used. At high peak power, these phase modulations can convert into intensity modulations by non-linear optical processes. This in turn can lead to loss in energy on target via many well known mechanisms. In some extreme cases damage to optical components downstream of the source of the modulation can occur. The NIF baseline design [5,6] requires 192 beamlines containing many large optical elements such as laser slabs, KDP crystals, mirrors, polarizers, lenses and windows. In all, approximately 7,000 large aperture optical components

are required. The wavefront requirements of optical components in the NIF depend on their location and function; i.e. whether the an element is transmissive or reflective, what fluence is incident on the part and whether the element encounters the first or third harmonic beam. The physics of the design further dictate three regimes of spatial scale length that are important. These regimes are:

i. short scale, or" micro roughness" having scale lengths < 0.12 mm,
ii. mid-spatial scale, with scale lengths from 0.12 to 33 mm and
iii. long scale, corresponding to optical figure / curvature having scale lengths > 33 mm.

Figure 4 is a matrix used to guide the metrology effort. Listed in the left-hand column are the major optical components; across the top are three scale length regimes. Entries in the matrix indicate the predominant loss mechanism or threat to laser system performance. The priority associated with the need for the data for modeling purposes is also indicated. Shaded entries indicate measurements completed.

2.4 Results - examples of wavefronts

A primary use of the data described here is beam propagation modeling, therefore care was taken to measure transmissive parts at use angle. That data is reported as single-pass transmitted wavefront. On the other-hand, reflected wavefronts are generally measured at near normal incidence, when used for modeling purposes the reflected wavefronts must be corrected to the use angle condition. This data is reported as reflected wavefront.

Figures 5 illustrates the test configuration used to measure the transmitted wavefront of laser slabs. The part is placed at Brewster's angle (Θ_{B1}) in the Fizeau interferometer cavity. The transmitted wavefront is measured for this configuration, the transmitted wavefront for the part is calculated by subtracting the wavefront of the empty cavity. Examples of the transmitted wavefront observed in laser slabs are shown in Figure 6a, b and c. These phase maps were measured with 38 mm square test apertures, to maximize the detection of features with 1 - 10 mm scale length. Figure 6a is a relatively random wavefront, while Figures 6b and c illustrate two forms of modulation that are sometimes observed.

Figures 7 illustrate the test configuration used to measure lenses in transmission. Full aperture measurement of NIF proto-type lenses is not possible in the Fizeau configuration due to their long focal length. In transmission, the cavity length must be chosen to place the focal point of the transmission sphere at the back focal spot of the lens. The central portion of the wavefront can be measured howerver, as shown in Figure 7. An example of modulation detected in the transmitted wavefront of an f/15 aspheric spatial filter lens is shown in Figure 8. Full aperture measurement of the transmitted wavefront is generally be made using unequal path laser interferometer (LUPI). Such measurements are made by the lens fabricators.

The reflected wavefront from lenses is not of direct interest to us for propagation modeling. Lens surface structure is primarily important as it affect the transmitted wavefront. The ability to separate bulk and surface effects is important however when the fabrication process is under

study. Then, a test configuration such as that shown in Figure 9 a and b can be used to measure the reflected wavefront. Once again, due to the large aperture and long focal length of proto-type lenses, only a sub-aperture can be measured (any sub-aperture can be measured, not just the central portion, by tipping the lens about the optical axis). In reflection, the focal point of the transmission sphere must coincide with the radius of curvature of the surface being tested. To detect very short scale length surface features, an interference microscope must be used. Very short features detected on the surfaces of spatial filter lens with an interference microscope are shown in Figure 10.

3. WAVEFRONT ANALYSIS

3.1 Calculation of phase

Modern phase shifting interferometry is highly evolyed. The optical technique of phase shifting traces its roots to work in the '60s, an early summary was written by Crane [7]. Data analysis is discussed more recently, in a review of algorithms by Creath [8]. Commercial Fizeau interferometers are currently available with apertures as large as 450 mm (18"). Custom instruments with slightly large aperture are also possible [9]. Two methods are used to calculate the phase of the wavefront: the "phase stepping" and the "phase ramping" (aka: "integrating bucket") methods. The specific method and algorithm by which the phase is determined is generally a proprietary attribute of commercial instruments. However, ithe porcess can be easily explained for the "4 step algorithm". The intensity at each pixel of the detector has the form:

$$I_{pixel} = a + b\cos(\Theta)$$

where "a" is a constant, "b" is the fringe contrast or visibility and Θ is the phase. The phase at each pixel is measured four times. Phase increments of $\pi/2$ separate each measurement:

$I_1 = a + b\cos(\Theta)$,
$I_2 = a + b\cos(\Theta + \pi/2) = a - b\sin(\Theta)$,
$I_3 = a + b\cos(\Theta + \pi) = a - b\cos(\Theta)$ and
$I_4 = a + b\cos(\Theta + 3\pi/2) = a + b\sin(\Theta)$.

Then the phase at each pixel is:

$$\Theta = \arctan\left[(I_4 - I_2) / (I_1 - I_3) \right].$$

The "integrating bucket" method is most often implemented because a settling time inherent in the "phase stepping" method is eliminated. In addition, the number of "buckets" of phase data collected isn't usually four, but another number optimized to enhance signal-to-noise for specific instrument and environmental conditions. Once the phase at each pixel is calculated, phase ambiguities are removed and the wavefront is constructed by connecting data points. For reliable

removal of discontinuities, the phase must not change by > $\lambda/2$ between adjacent pixels. This requirement determines the maximum vertical step height and the maximum slope that can be resolved by this technique.

After the wavefront has been constructed, the data can be analyzed by various methods. This can include "curve fitting" and filtering so that specific wavefront attributes (shapes or spatial components) can be observed.

3.2 Data analysis

In the past wavefronts of ICF optical components have been described for a specific aperture in terms of P-V, gradient and rms. The performance of high peak power laser systems, such as the NIF, is dominated by diffraction and non-linear optical effects caused by the interaction of the collimated, high intensity. coherent (narrow bandwidth) beam with materials and interfaces which can impart periodic modulation onto the propagating wavefront. These effects dictate three regimes of scale length as discussed in "Metrology requirements."

Traditionally, wavefront shape has been expressing by fitting the wavefront in terms of Zernicke polynomials [10]. Zernicke polynomials correctly describe only circular apertures, since the polynomials form an orthogonal set only for this aperture shape. Furthermore, Zernicke analysis treats only low spatial frequency wavefront aberrations commonly referred to as "shape" or "curvature"; the classical third order (Seidel) abberations are directly related to the first eight polynomials. Mid-spatial scale and high frequency error are expressed only as "residuals" of the polynomial fit. Zernicke analysis can not take advantage of all the high resolution data available because there are a limited number of polynomials (37) to fit. The residual of the Zernicke fit can not be reduced below that calculated based on the "complete" or 37 term fit. These severe limitations on the use of Zernicke analysis suggests that an alternative method be used.

Fourier analysis of the high spatial resolution wavefront data produced by modern interferometers is appropriate to ICF modeling needs. Fourier analysis is potentially a very powerful method of wavefront analysis for NIF components. There is no implied limitation on either the aperture shape or the spatial resolution. Fourier wavefront analysis is limited only by the spatial bandwidth of the data available.

3.3 Physical interpretation of the Power Spectral Density

The Power Spectral Density (PSD) is calculated from the amplitude of frequency components in the wavefront Fourier amplitude spectrum. The PSD is a physically significant figure-of-merit for expressing the wavefront structure or shape. The PSD directly yields information about:

i. periodic wavefront structure through the appearance of peaks in the PSD,
ii. the average squared roughness (RMS) of the wavefront for any frequency band for which data is available, and
iii. the intensity and distribution of scattered light.

The PSD is widely used by workers in the precision metrology field. Calculation of this function is straight-forward in principle [11] however care must be exercised when using commercial analysis software. The optical PSD, was developed during the '70s by those working to quantify optical scatter [12] and relate it to surface roughness of optical surfaces. The PSD was first formulated by Church [13, 14] and later proposed by Janeczko [15] to specify surface roughness of infrared materials. In 1-D, the magnitude of the PSD for a given frequency, ν_i, is given by:

$$PSD(\nu_i) = A(\nu_i)^2 / (\Delta\nu),$$

where $A(\nu_i)$ is the Fourier amplitude for frequency ν_i.

If repetitive modulation is present in the wavefront, peaks will appear when the PSD is displayed vs. frequency see Figures 11 - 14). These peaks correspond to large Fourier components at the frequency of the wavefront modulation. The integral of the PSD over a frequency range yields the RMS roughness of the wavefront. When the Fourier pair consist of distance (or scale length) and spatial frequency; Parseval's theorem [16] for Fourier series becomes a statement of the rms:

$$\int_{\nu_0}^{\nu} A(\nu_i)^2 \, d\nu = \sum_i c_i^2 .$$

Then:

$$\int_{\nu_0}^{\nu} PSD(\nu_i) \, d\nu = (RMS)^2 .$$

The RMS is valid over the same frequency interval as the PSD.

Further significance of the PSD comes from the physics of small angle scattering [17]. Fourier analysis reconstructs the measured wavefront by calculating an equivalent series sinusoidal terms, each with amplitude $A(\nu)$. The effect of such a surface on a propagating beam is to cause diffraction from the sinusoidal components. The scattered light will be diffracted according to the grating equation. If the amplitude of the gratings, $A(\nu)$, is much less than the wavelength of the light (as for NIF optics), then the intensity of the scattered light in each order is:

$$\text{scattered intensity} \sim (\text{grating amplitude})^2 .$$

So the PSD is proportional to the scattered intensity and direction. The PSD can be used to calculate the intensity distribution in a propagating beam [18].

3.4 1-D analysis :

A one dimensional PSD is sufficient to characterize a part if the wavefront structure is:

i. isotropic, then all directions are equivalent,
ii. "simple" (single frequency and unidirectional) and easy to observe (large magnitude) or

iii. only specified in one dimension or one direction on the part.

In these situations the direction of interest is specified by design or determined by the wavefront.

The Fourier analysis capability of the software that supports commercial instruments is limited. These analysis packages allow multiple profiles to be taken in the wavefront, but do not averaging them to reduce noise. Another potential concern are the assumptions made in the Fourier analysis, particularly when the profile selected does not contain a number of data point equal to an intergral power of 2. In this case, the data often will be "padded" with zeros., often the analyst is not aware. Data "padding" can cause aliasing and erroneous frequencies in the Fourier spectrum. In order to better control the assumptions made in the Fourier analysis, we have developed our own software using a graphics based software package, Interactive Data Language (IDL®).

We have written a macro program that analyzes the wavefront data in the following steps, it

i. measures multiple (ten) profiles,
ii. calculates the PSD for each using a Hanning window on the profiles to suppress the effect of finite profile length,
iii. averages the PSDs and display the averaged result.

Examples of this capability applied to wavefront data are shown in Figure 11 and 12. Signal averaging reduces the noise in a single profile by taking multiple data sets to calculate a meaningful 1-D PSD. Two phase maps measuring 38 mm square are shown in Figurea 11a and 12a. A direction on the wavefront is chosen by selecting a "line-out" with a given physical length, L_0. The 1-D profiles are shown in Figures 11b and 12b. The data is then processed by a Fast Fourier Transform (FFT) routine. Raw PSDs are shown in Figures 11c and 12c. The averaged PSDs are shown in Figures 11d and 12d. The discrete Fourier transform [19, 20] defines the following characteristics in the amplitude spectrum :

$\nu_i = i/L_0$, where i is an integer and L_0 is the length of the "line-out" selected (including "padded zeros" if necessary)

ν_0, the lowest frequency, equal to $1/L_0$,

ν_{max}, the highest frequency, equal to (2x pixel or image resolution)$^{-1}$, also known as the Nyquist limit

$\Delta\nu$, the increment between frequencies, equal to $1/L_0$

The units of PSD in 1-D are (length)^3, in the examples used here: (Angstrom)^2 x (millimeter). The PSD is often expressed in log-log form to shown the wide range of amplitude variation in the Fourier spectrum [13].

3.5 2-D PSD

A two dimensional PSD is necessary to fully characterize the wavefront if:

i. the wavefront is anisotropic,
ii. the structure in the wavefront isn't clearly visible (low magnitude) or if the shape of the structure is complex (more than one dominant frequency component or directions), or
iii. the part must be characterized in 2-D.

In general these are characteristics of wavefronts of NIF optical components. There is no preferred scattering direction about the propagation direction in the optical system, scattering and amplitude modulation is of concern equally in all directions. Therefore, wavefront modulations must be quantified uniformily in 2-D about the beam propagation direction.

Using IDL ® we have written software to calculate the PSD in 2-D. Analysis in 2-D makes use of the entire data set (> 300, 000 data points), this automatically accomplishes the signal averaging done by multiple "line-outs" in 1-D. Figures 13a and 14a shows the phase maps used. Figures 13b and 14b show that data filtered with a Hanning window. The Hanning window is a low frequency filter (cosine^2) used to prevent aliasing at low frequencies. Figure 13c and 14c display the calculated PSD, log scale. Finally, Figures 13d and 14d show a PSD surface, plotted on a linear scale. The power of the 2-D analysis is apparent from these examples, complex features over-looked by the simpler 1-D analysis are clearly resolved in 2-D. We intend to extend our work in 2-D analysis as part of the maturing beam modeling and propagation efforts in support of the NIF.

4. ACKNOWLEDGEMENTS

This work has been conducted in support of optical component development efforts in the ICF Program at the Lawrence Livermore National Laboratory. The authors express their gratitude to many individuals for assistance and insight concerning this work, including: D. M. Aikens, J. L. Atherton, J. M. Auerbach, A. Demiris, R. E. English, J. T. Hunt, M. Kellam, R. T. Maney and K. R. Manes. This work was performed under auspices of the U S Department of Energy by the Lawrence Livermore National Laboratory under contract No. W-7405--ENG-48.

5. FIGURES

1a. Schematic drawing of the GPIxp interferometer layout
1b. The GPIxp 102/457 mm (4"/18") interferometer (photos)
2. A 38 mm square phase map of the reflected wavefront of crystal LL-8-2: P-V = 0.086 λ, @ 633 nm
3 Ideal, or detector limited, frequency bandwidth vs. aperture diameter and detector element count.
4 Metrology matrix for NIF optical components
5 Test configuration for laser slabs at Brewster's angle
6 38 mm square aperture transmitted wavefronts from laser slab
6a. A relatively random, unmodulated wavefront,

P-V = 0.19 λ, @ 633 nm

6b. A wavefront exhibiting modulation primarily in 1-D, magnitude is l/70 with a scale lengths from 5 - 7 mm, P-V = 0.35 λ, @ 633 nm

6c. A wavefront exhibiting complex (curved, multiple frequencies) modulation, magnitude is l/100 with scale lengths from 5 - 7 mm,
P-V = 0.17 λ, @ 633 nm

7. Test configuration for measuring the transmitted wavefront of lenses

8. Transmitted wavefront modulation detected in a spatial filter lens, P-V = 0.037 λ ,@ 633 nm

9. Test configuration for measuring the reflected wavefront of lenses

10. Short scale length surface features detected on both the spherical and aspheric surfaces of a spatial lens

10a. Surface #1 aspheric, magnitude of modulation 9.1 nm,
over-all P-V = 35.5 nm

10b. Surface #2 spherical, magnitude of modulation 10.6 nm,
over-all P-V = 27.6 nm

11. An example of 1-D Fourier analysis of the reflected wavefront from a diamond turned KDP crystal surface (same data as Figure 2)

11a. Phase map with multiple profiles defined

11b. Profiles of phase height vs. position, taken from the map of Figure 11a

11c. Individual PSDs for each profile shown in Figure 11b

11d. The averaged PSD

12: Example of 1-D Fourier analysis of a transmitted wavefront

12a. Phase map with multiple profiles defined

12b. Profiles of phase height vs. position, taken from the map of Figure 12a

12c. Individual PSDs for each profile shown in Figure 12b

12d. The averaged PSD

13: Examples of 2-D Fourier analysis of a reflected wavefront (same data as Figures 2 and 11)

13a. Phase map data

13b. Phase map with Hanning window applied

13c. PSD calculated in 2-D

13d. PSD surface

14. Examples of 2-D Fourier analysis of a transmitted wavefront (same data file as Figure 12)

14a. Phase map data

14b. Phase map with Hanning window applied

14c. PSD calculated in 2-D

14d. PSD surface

6. REFERENCES

[1] W. Augustyn, et al; *"An automatic interference pattern processor with interactive capability"* Proc. of the SPIE vol. 153 p. 146 1978

[2] Wyko Corp., Phase Shift Technology , (both in Tucson Ariz.) and Zygo Corp. (Middlefield Conn.) sell instruments of this kind.

[3] There are several sources for "special" arrays, EG&G, Spectra Source and Dalsa are examples.

[4] E. L. Church et al; *"Direct comparison of mechanical and optical measurements of the finish of precision machined optical surfaces"*, Optical Engineering vol. 24 no. 3 p. 388 May/June 1985

[5] National ignition facility conceptual design report, UCRL-PROP-117093, May 1994.

[6] Energy & Technology Review - December 1994: "The National Ignition Facility": UCRL-52000-94-12, published by UC Lawrence Livermore National Lab, available from: National Technical Information Service, US Department of Commerce, 5285 Port Royal Rd., Springfield Va., 22161

[7] R. Craane; *"Interference phase measurement"*, Applied Optics vol.8 no. 3 p. 538 March 1969

[8] K. Creath; *"Phase Measurement Interferometry Techniques"*, chapter V in Progress in Optics XXVI edited by E. Wolf: 1988 North-Holland Press Inc.

[9] Wyko, Zygo, Phase Shift Technology and others are considering large aperture commercial instruments.

[10] C-J. Kim, R. R. Shannon; *"Catalog of Zernicke Polynomials"*, chapter IV in Applied Optics and Optical Engineering - volume X edited by R. R. Shannon and J. C. Wyatt: Academic Press Inc. 1987

[11] J. M. Elson, J. M. Bennett; *"Calculation of the power spectral density from surface profile data"*, Applied Optics vol. 34 no. 1 p.201, January 1995

[12] J. M. Bennett and L. Mattsson; *"Scattering Theories and Surface Statistics"* , chapter 4 in Introduction to Surface Roughness and Scattering, published by, OSA: ISBN 1-55752-108-5, 1989

[13] E. L. Church et al; *"Direct comparison of mechanical and optical measurements of the finish of precision machined optical surfaces"*, Optical Engineering May/June 1985, vol 24 no. 3

[14] E. L. Church; *"Fractal Surface Finish"*, Applied Optics 27, 1518, 1988

[15] D. J. Janeczko; *"Power Spectrum Standard for Surface Roughness: Part I"*, Proc. SPIE Vol. 1165 Scatter from Optical Components (1989) p 175

[16] J. D. Gaskill; Linear systems, Fourier transforms and optics, p. 217, John Wiley and Sons 1978.

[17] J. C. Stover; *"Introduction to light scatter"* chapter 1 in Optical Scattering Measurement and Analysis, see discussion of small angle approximation and references: McGraw-Hill Inc., Optical and Electro-optical Engineering Series, 1990, ISBN 0-07061814-3

[18] G. Gallatin; *"Wavefront Power Spectrum and Scattering"* unpublished, currently with SVG Lithography Wilton, Conn.

[19] M. R. Spiegel; *"Fourier Series and Applications"*, chapter 2 in Theory and Problems of Fourier Analysis : Schaums' Outline Series McGraw-Hill Inc., 1991

[20] R. D. Strum, D. E. Kirk; *"Discrete Fourier Transform"*, chapter 7 in Discrete Systems and Digital Signal Processing: Addison-Weslet Publishing Co., 1989

Top view:

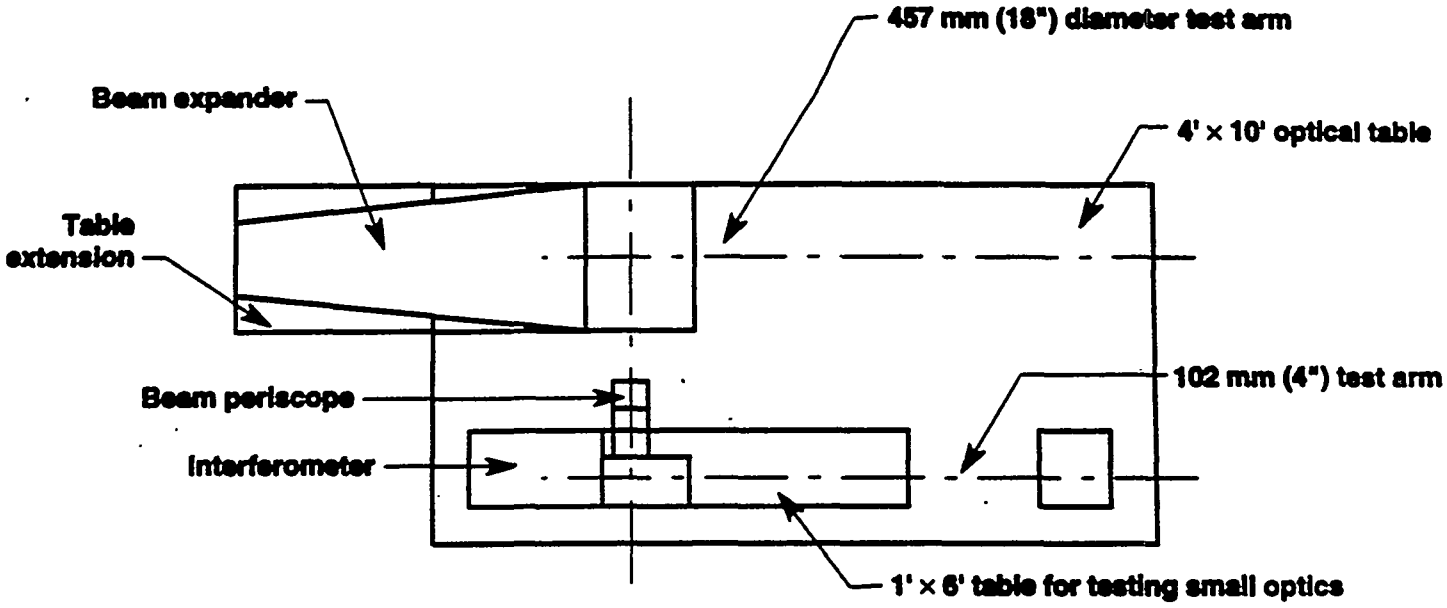

Elevation view:

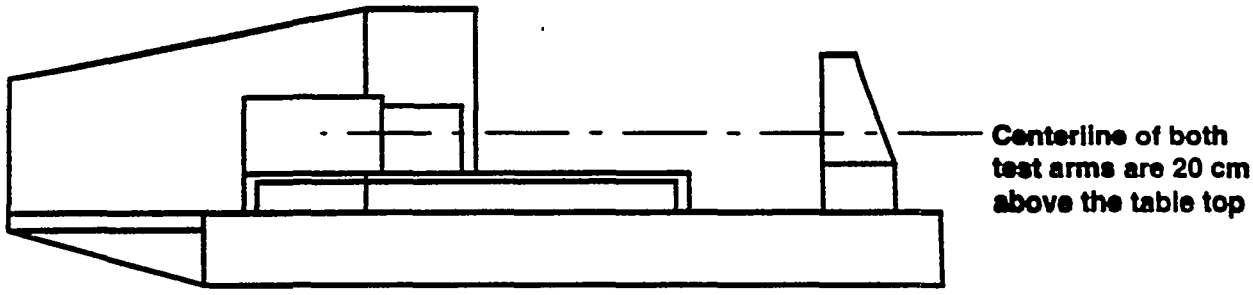

Figure 1a:
Schematic drawing of the GPIxp interferometer layout

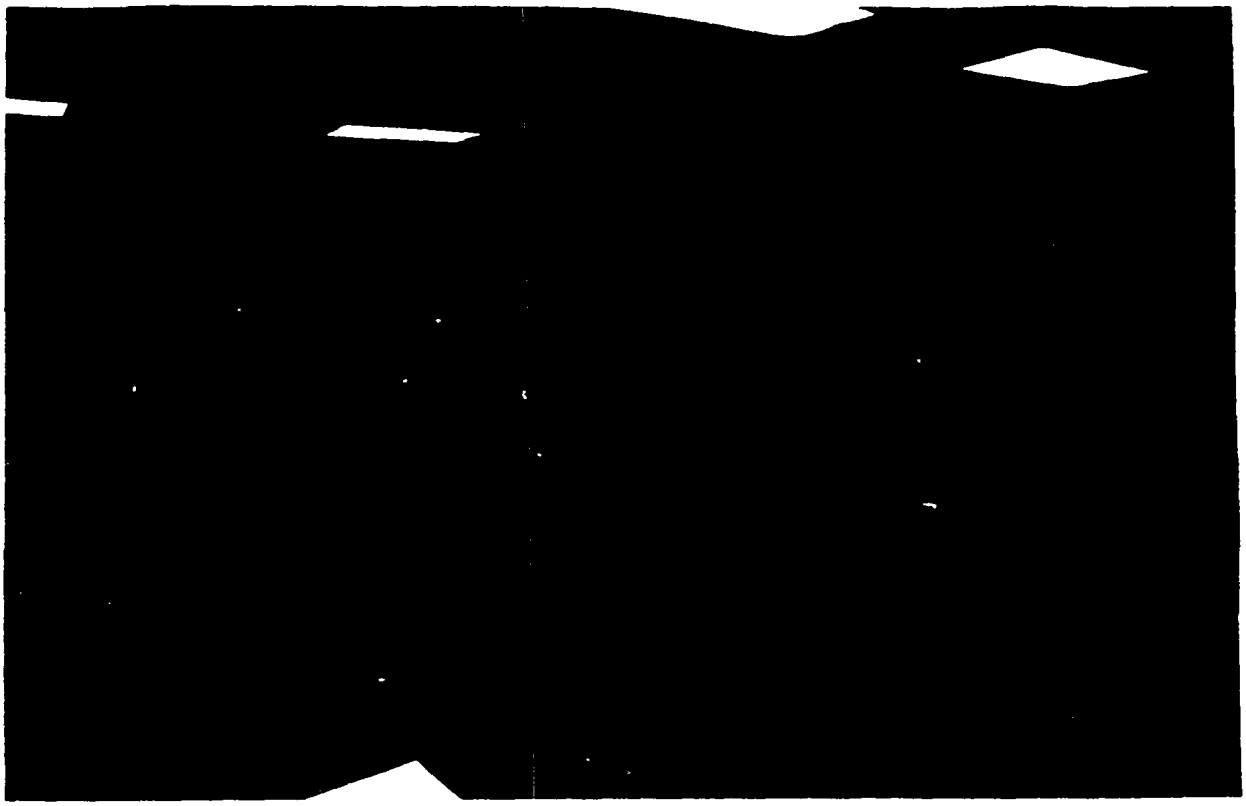

Figure 1b:
The GPIxp 102 / 457 mm (4"/18") interferometer (photos)

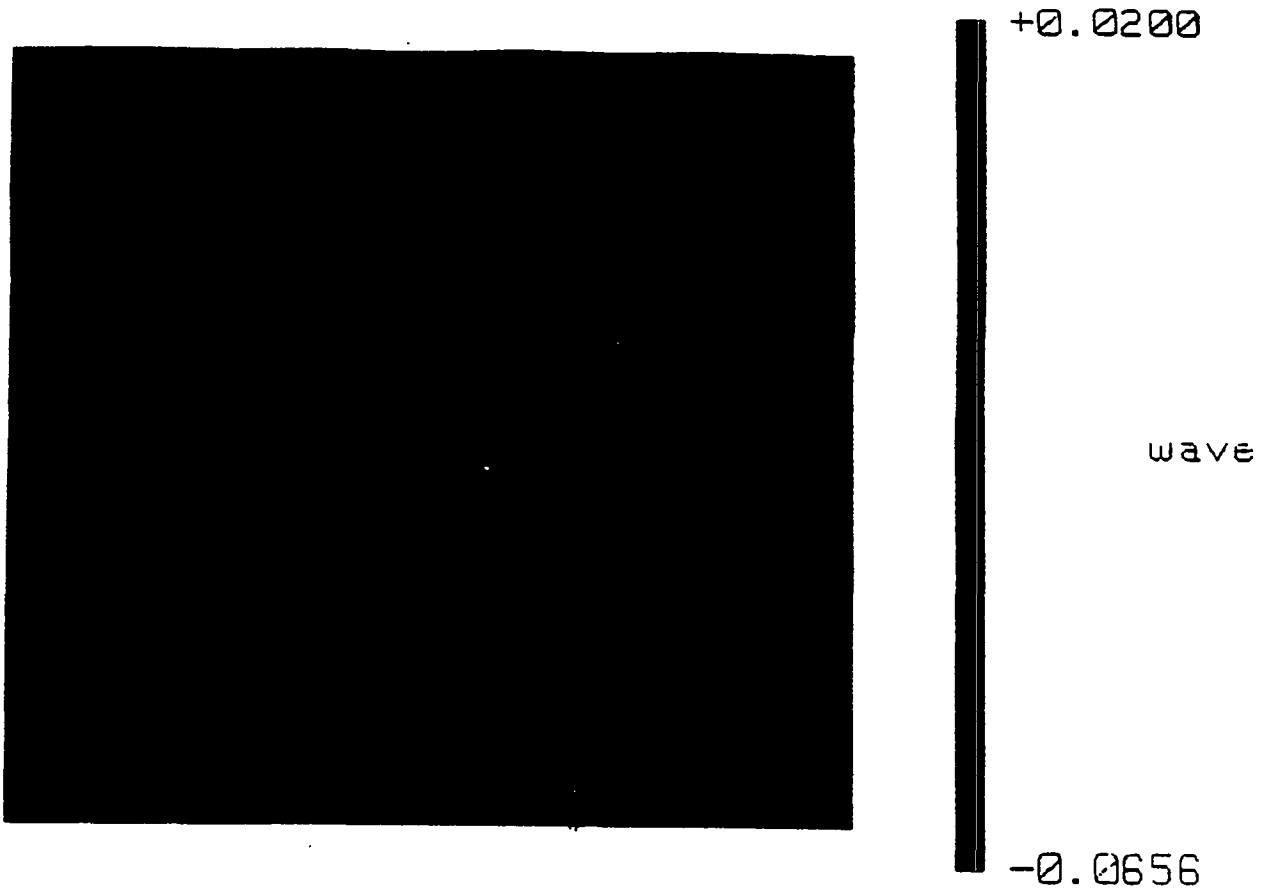

Figure 2:
A 38 mm square phase map of the reflected wavefront of crystal LL-8-2: P-V = 0.086 λ, @ 633 nm

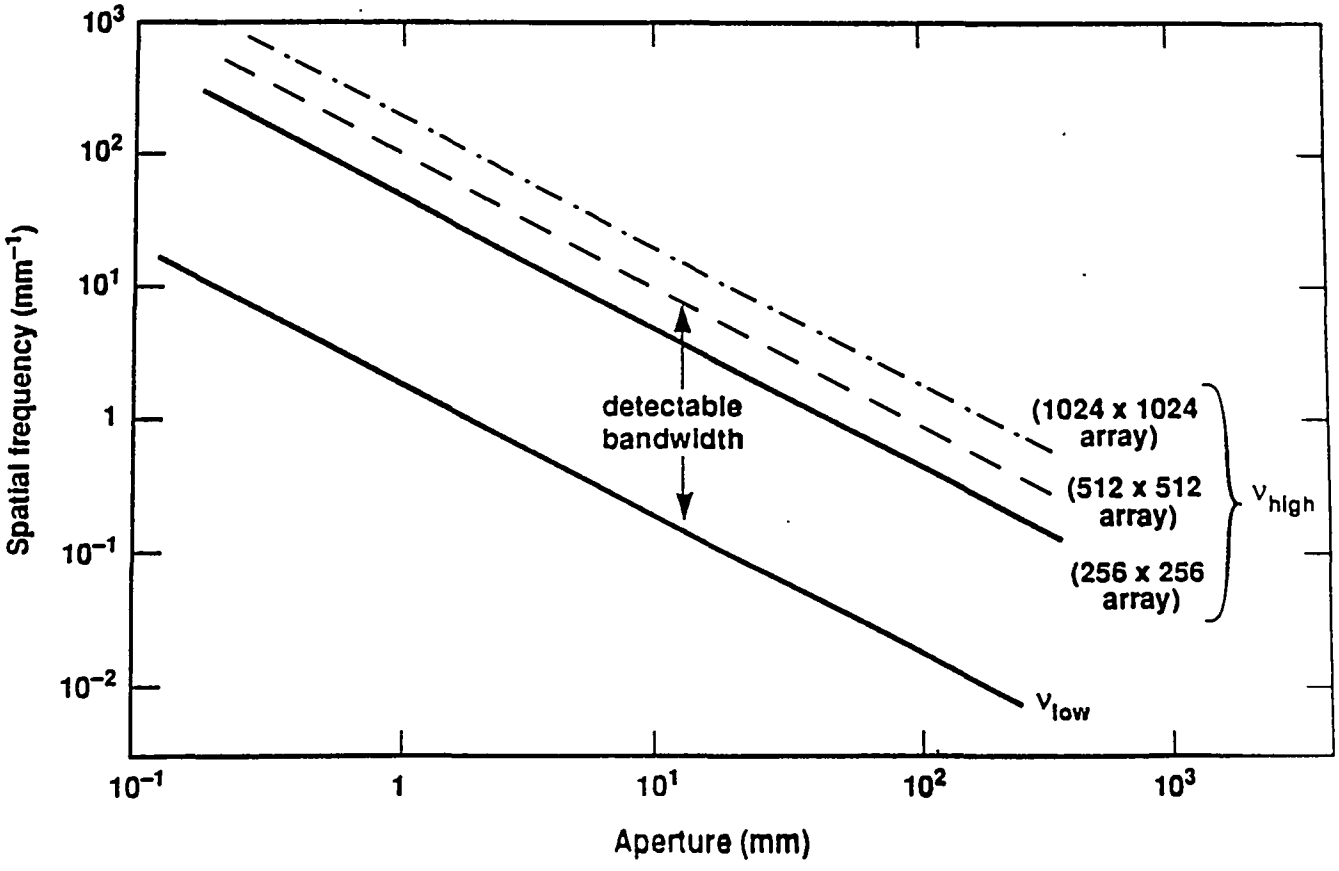

70-39-0894-3318pb01

Figure 3:
Ideal, or detector limited, frequency bandwidth vs. aperture diameter and detector element count.

optical component: *reason for concern - priority**	spatial wavelength measured, mm "roughness" < 0.12	"mid-spatial wavelengths" 0.12 - 33.0	"optical figure, curvature" > 33.0
laser slabs	energy loss -3	pin hole closure - 2 beam modulation, damage - 1	far-field modeling - 1
KDP crystals: Pockells cell	[illegible]	pin hole closure - 2 beam modulation, damage - 1	far-field modeling - 1
frequency conversion	energy loss - 3	beam modulation, damage - 1	beam modulation, damage - 1 conv. efficiency - 3
mirrors: cavity	energy loss - 3	pin hole closure - 1 beam modulation, damage - 1	far-field modeling - 1
transport/turning	energy loss - 3	beam modulation, damage - 1	far-field modeling - 1
polarizer	energy loss - 3	pin hole closure - 1 beam modulation, damage - 1	far-field modeling - 1
lenses: CSF	energy loss - 3	pin hole closure, energy loss - 2 beam modulation, damage - 1	far-field modeling - 1
TSF	energy loss - 3	beam modulation, damage - 1	far-field modeling - 1
Focus	energy loss - 3	beam modulation, damage - 1	energy loss - 3
windows: Pockells cell	energy loss - 3	pin hole closure - 2 energy loss - 2 beam modulation, damage - 2	[illegible]
gas box	energy loss - 3	beam modulation, damage - 2	[illegible]
debris shield	energy loss - 3	beam modulation, damage - 2	[illegible]
How measured ?			
Maxim 3D	40 x Fizeau	1x Fizeau	[illegible]
Mark IV / GPIxp	[illegible]	8 mm aperture 38 mm aperture	100 - 450 mm aperture
32" static fringe	[illegible]	[illegible]	full aperture

* priority: 1 - highest, 3 lowest
shaded entries indicate measurements have been made

Figure 4:
Metrology matrix for NIF optical components

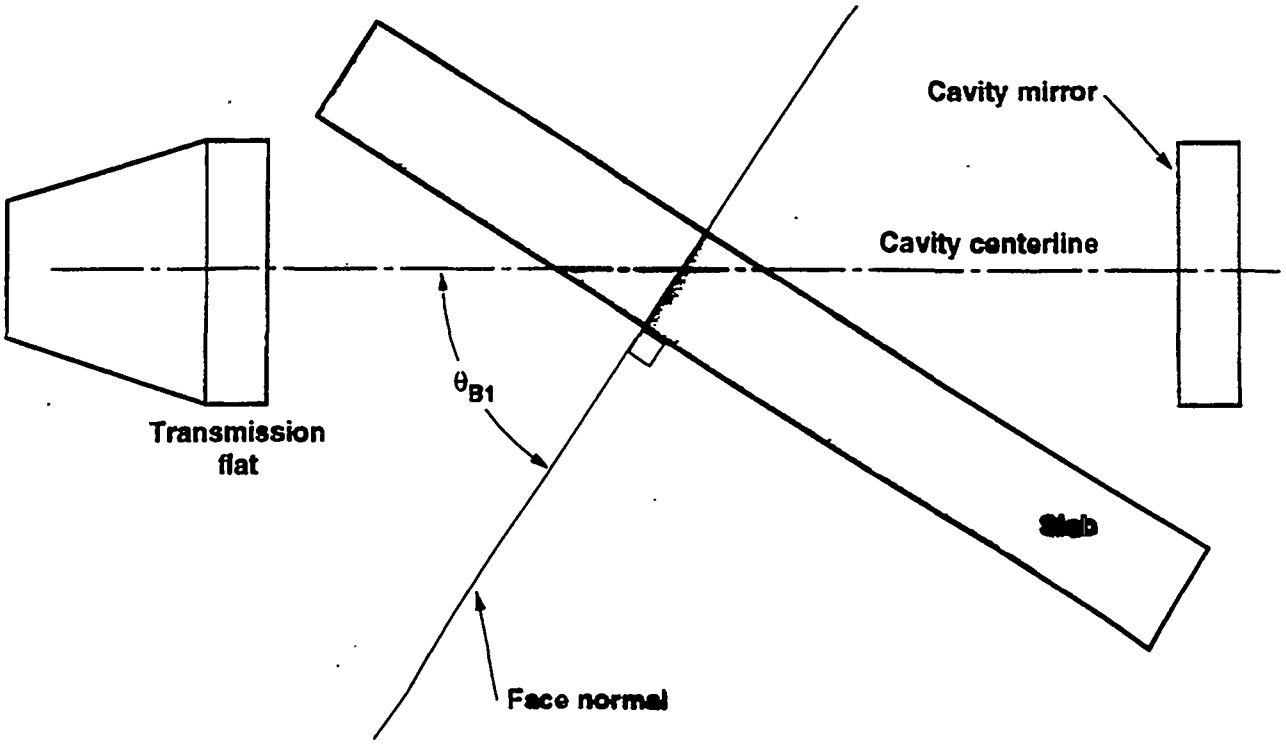

Figure 5:
Test configuration for laser slabs at Brewster's angle

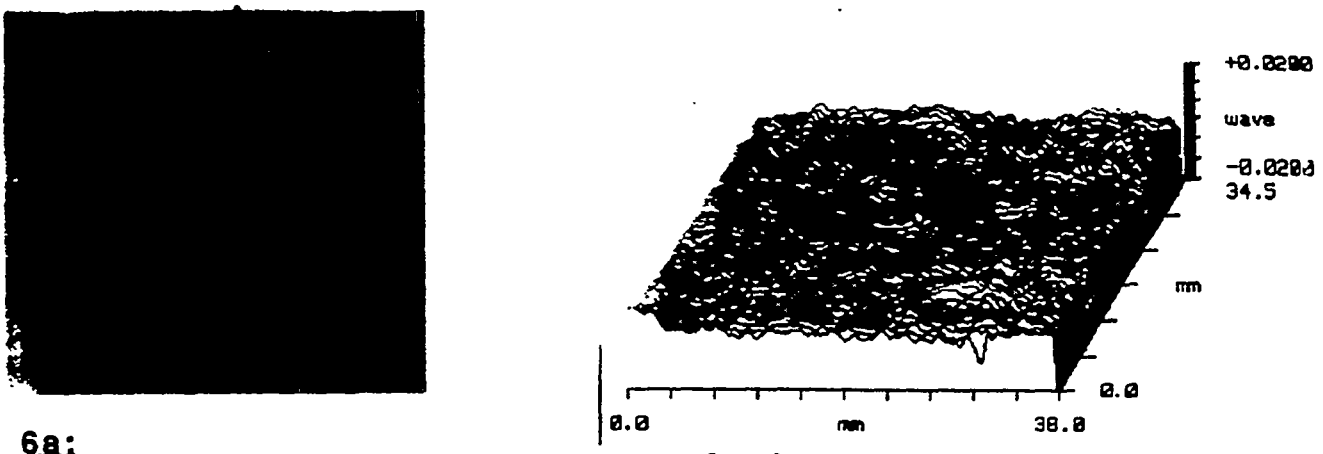

6a:
A relatively random, unmodulated wavefront,
P-V = 0.19 λ, @ 633 nm

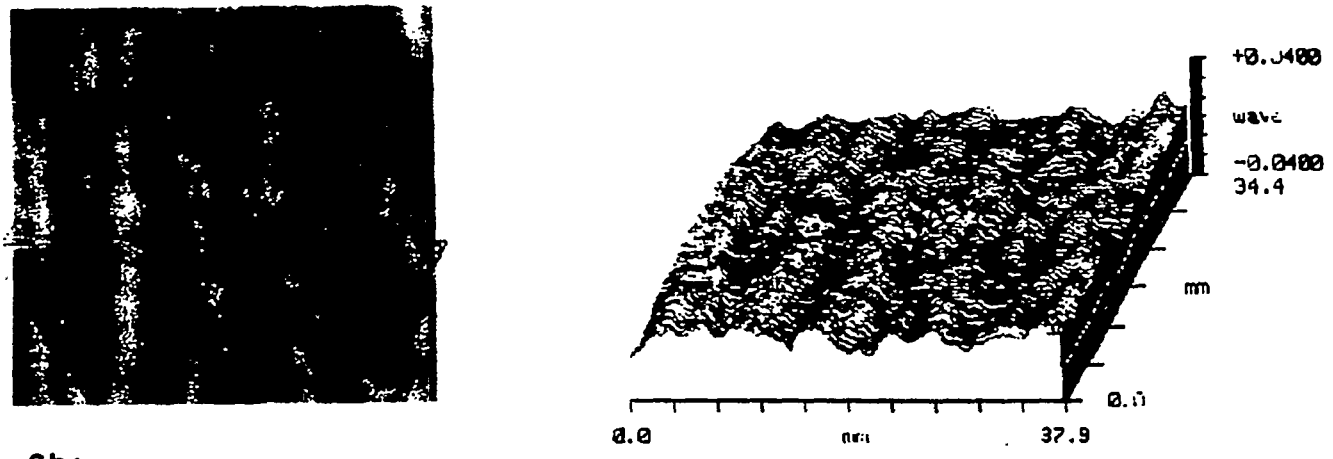

6b:
A wavefront exhibiting modulation primarily in 1-D, magnitude is λ/70 with a scale lengths from 5 - 7 mm, P-V = 0.35 λ, @ 633 nm

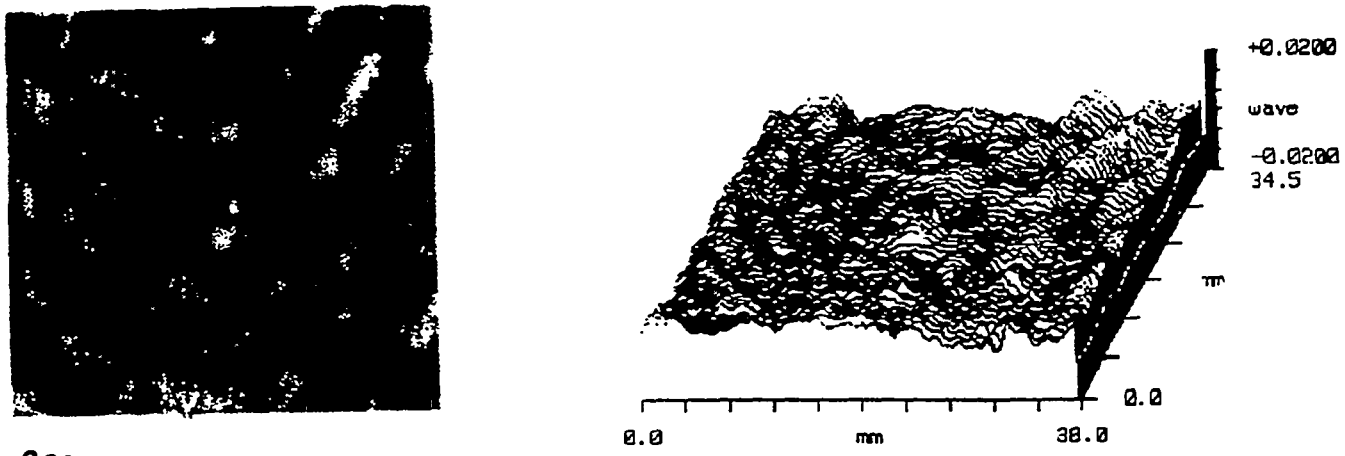

6c:
A wavefront exhibiting complex (curved, multiple frequencies) modulation, magnitude is λ/100 with scale lengths from 5 - 7 mm, P-V = 0.17 λ, @ 633 nm

Figure 6:
38 mm square aperture transmitted wavefronts from laser slabs

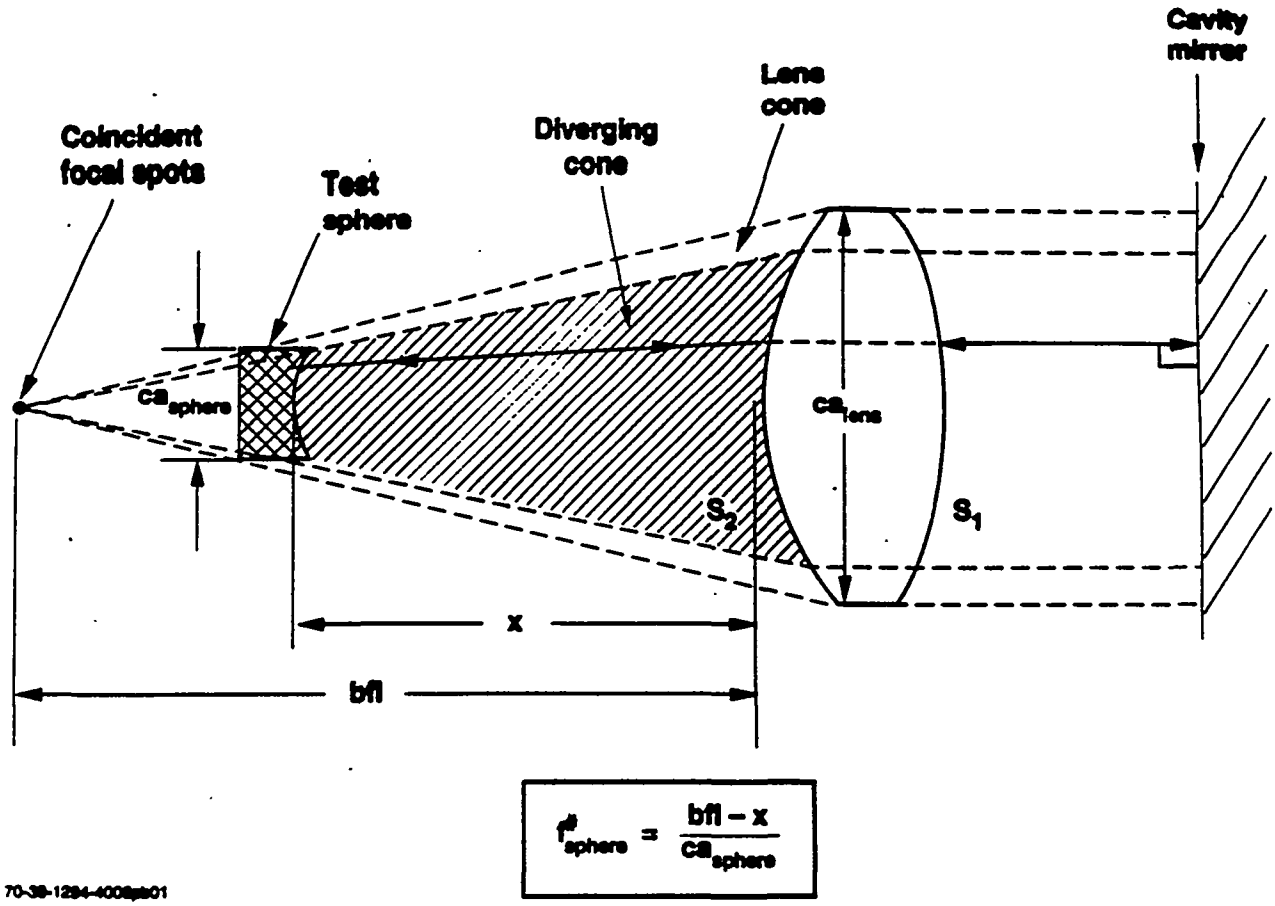

Figure 7:
Test configuration for measuring the transmitted wavefront of lenses

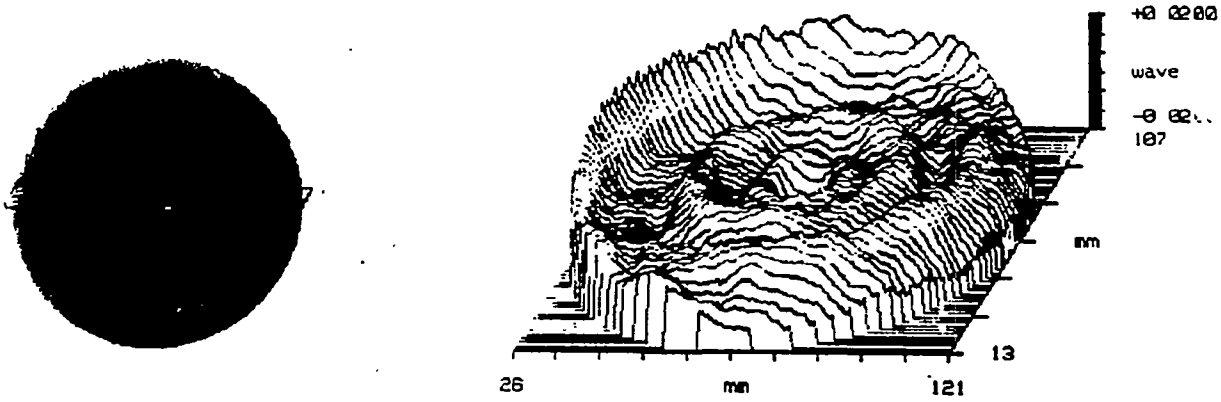

Figure 8:
Transmitted wavefront modulation detected in a spatial filter lens. P-V = 0.037 λ, @ 633 nm

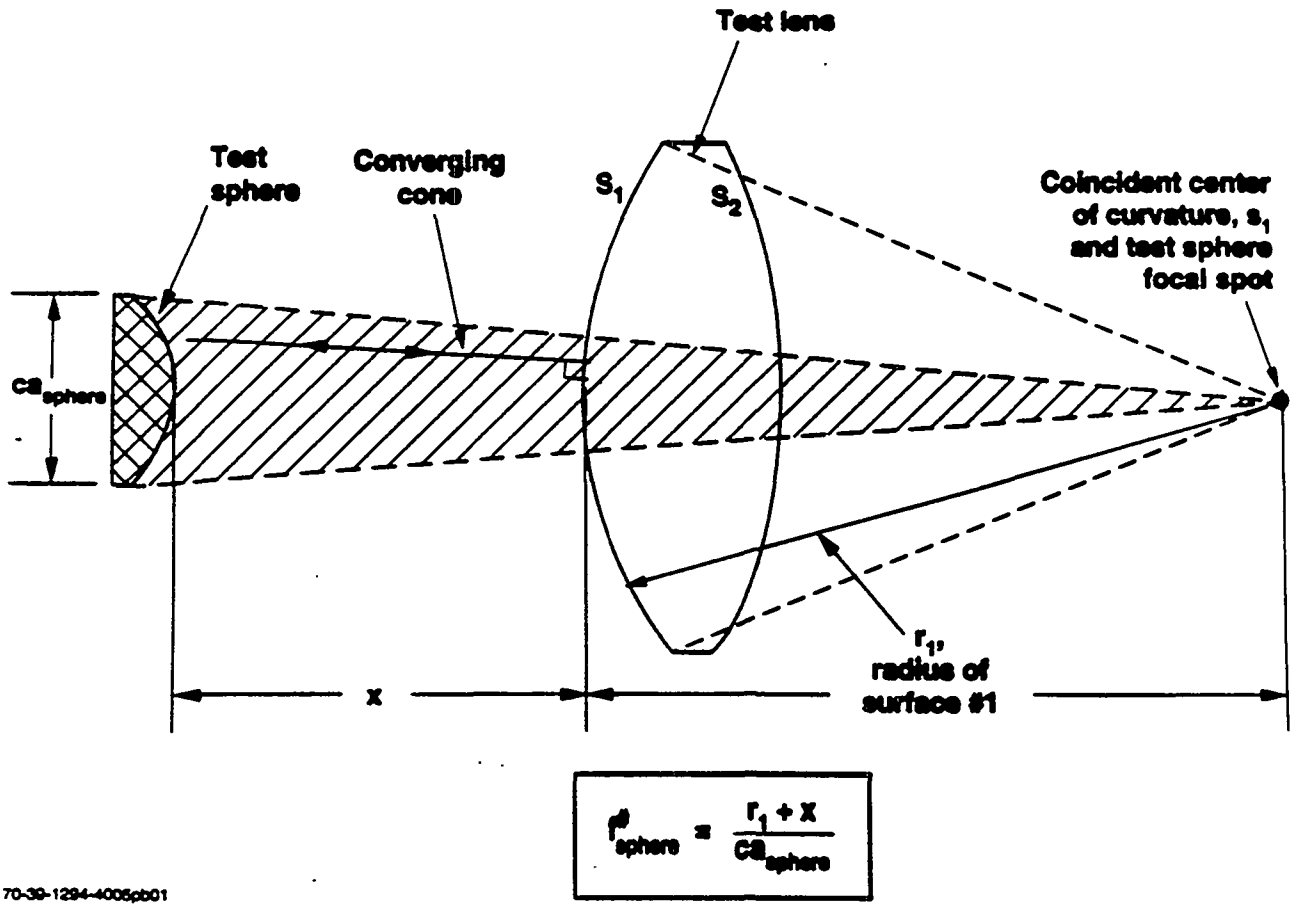

Figure 9:
Test configuration for measuring the reflected wavefront of lenses

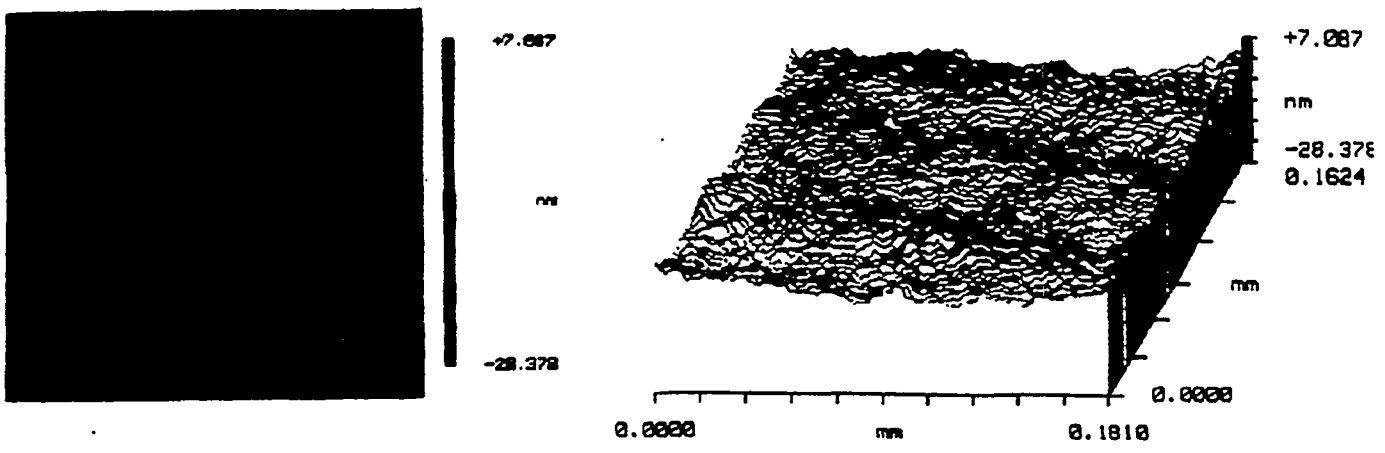

10a:
Surface #1 aspheric, magnitude of modulation 9.1 nm, over-all P-V = 35.5 nm

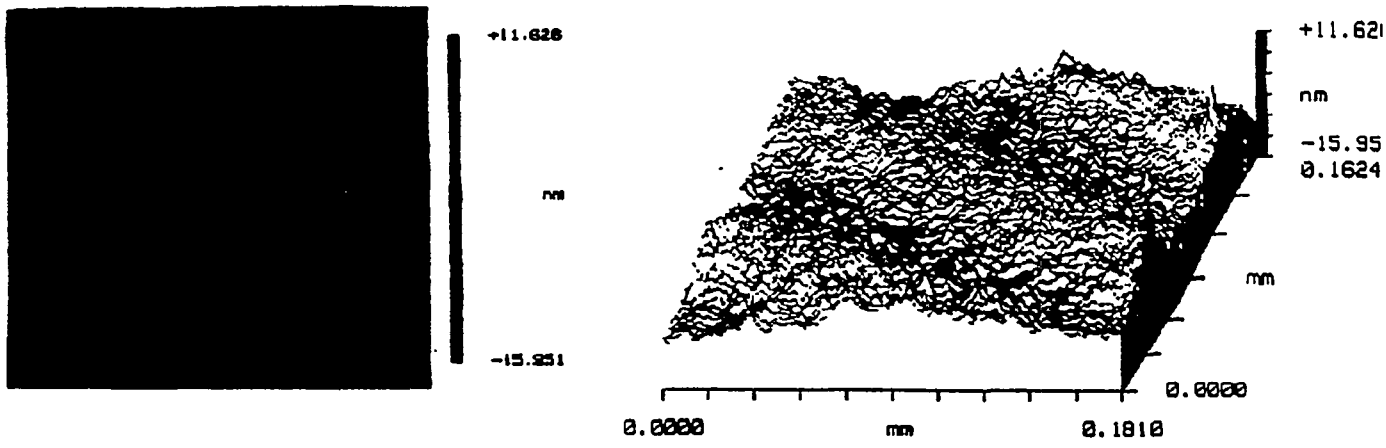

10b:
Surface #2 spherical, magnitude of modulation 10.6 nm, over-all P-V = 27.6 nm

Figure 10:
Short scale length surface features detected on both the spherical and aspheric surfaces of a spatial lens

11a:
Phase map with multiple profiles defined

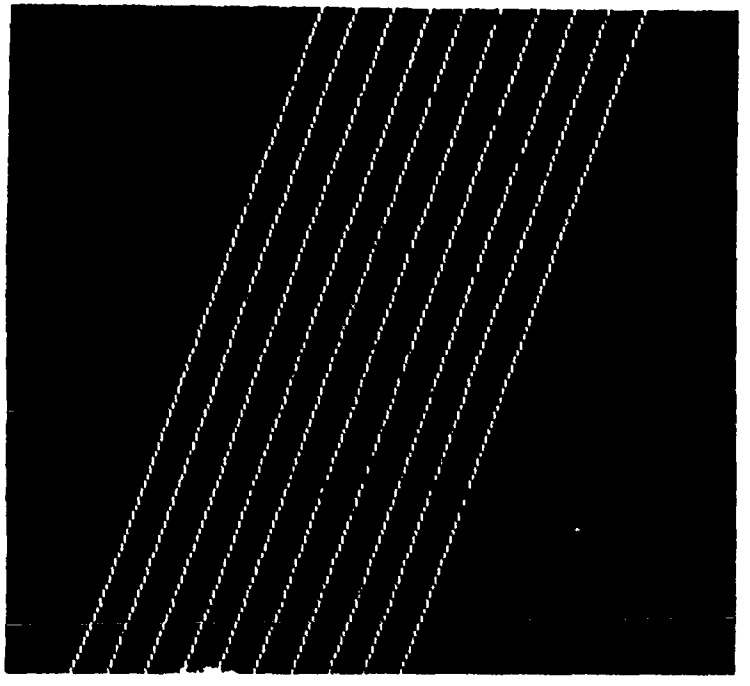

11b:
Profiles of phase height vs. position

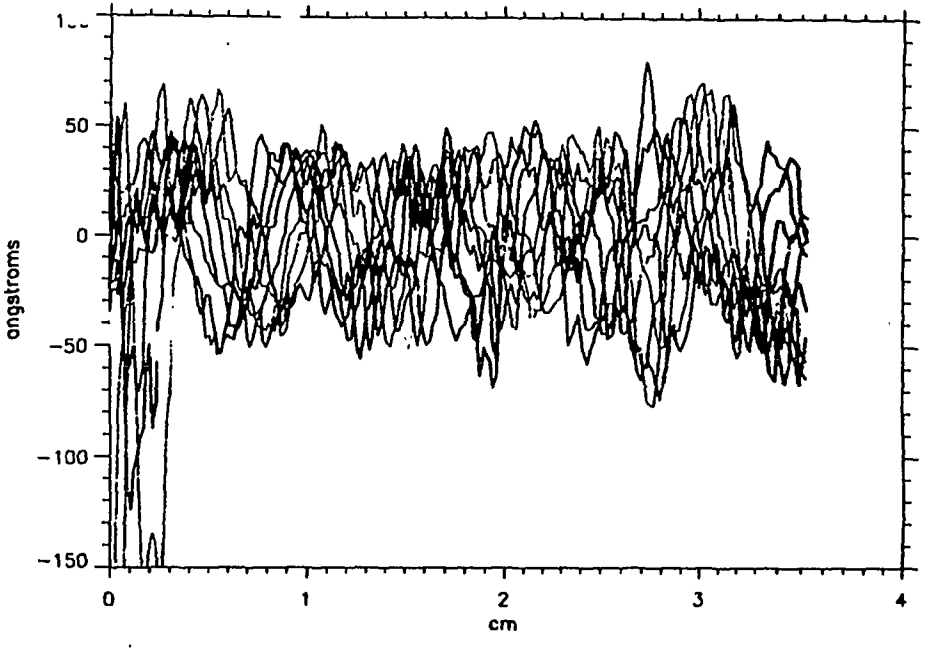

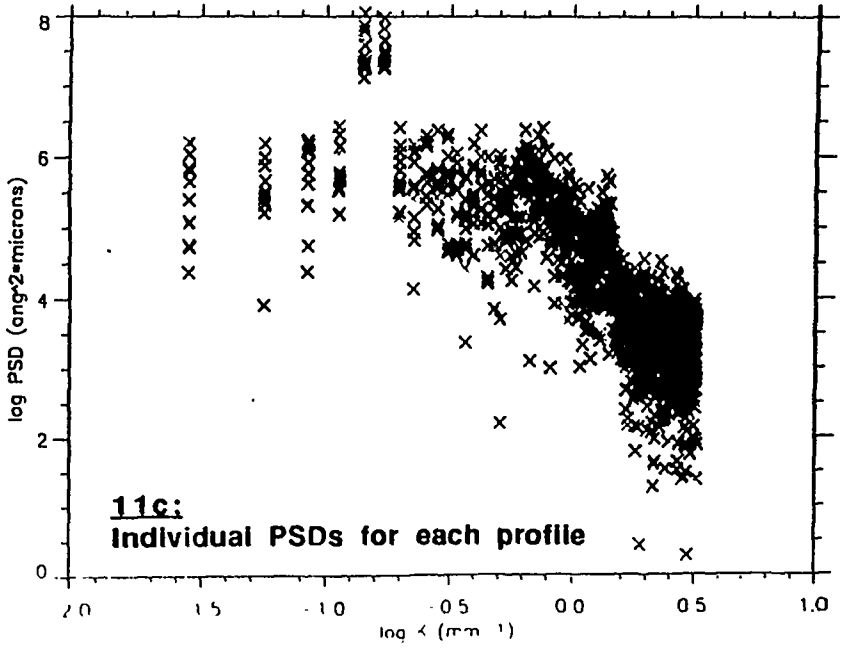

11c:
Individual PSDs for each profile

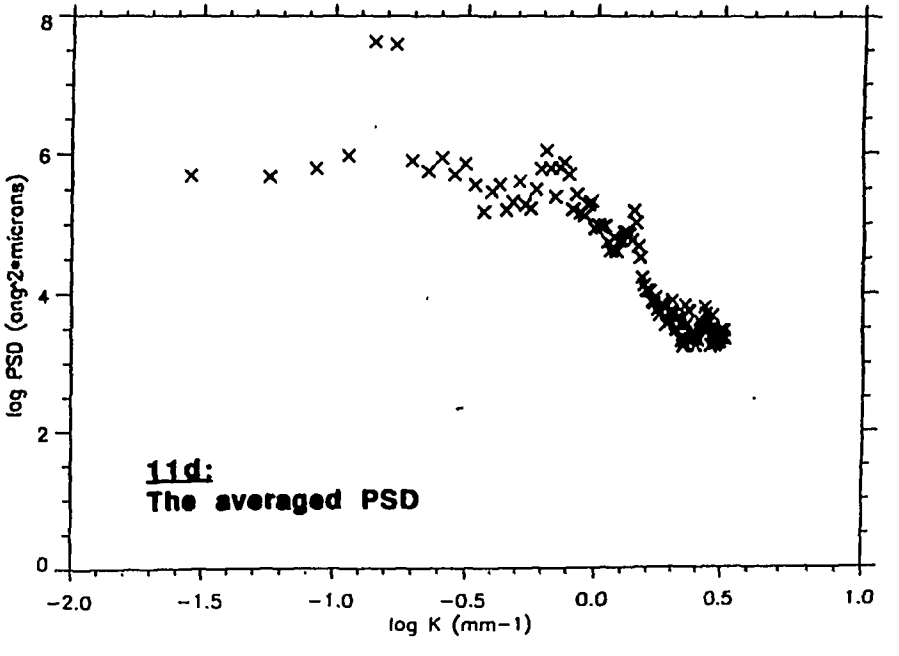

11d:
The averaged PSD

Figure 11:
An example of 1-D Fourier analysis of the reflected wavefront from

12a:
Phase map with multiple profiles defined

12b:
Profiles of phase height vs. position

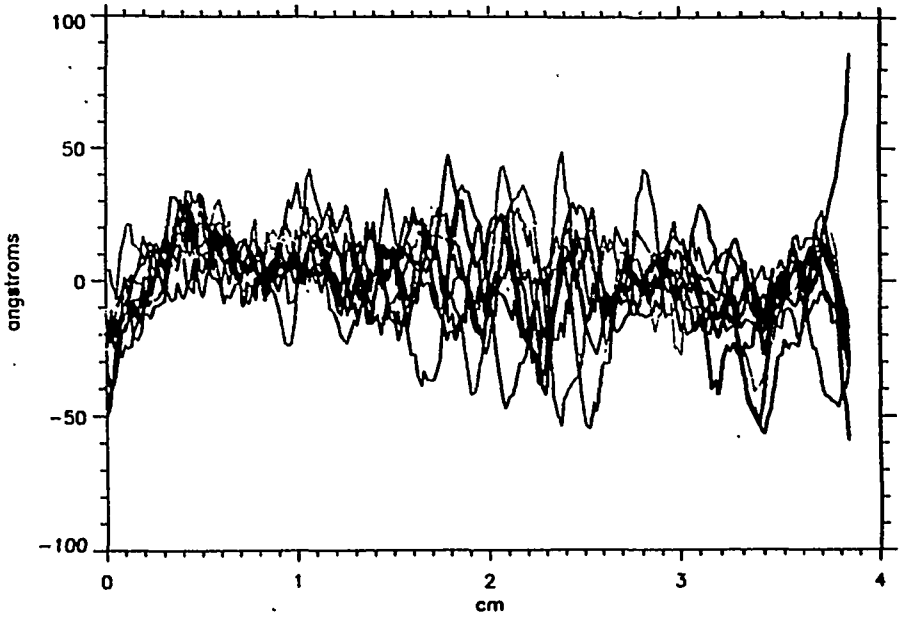

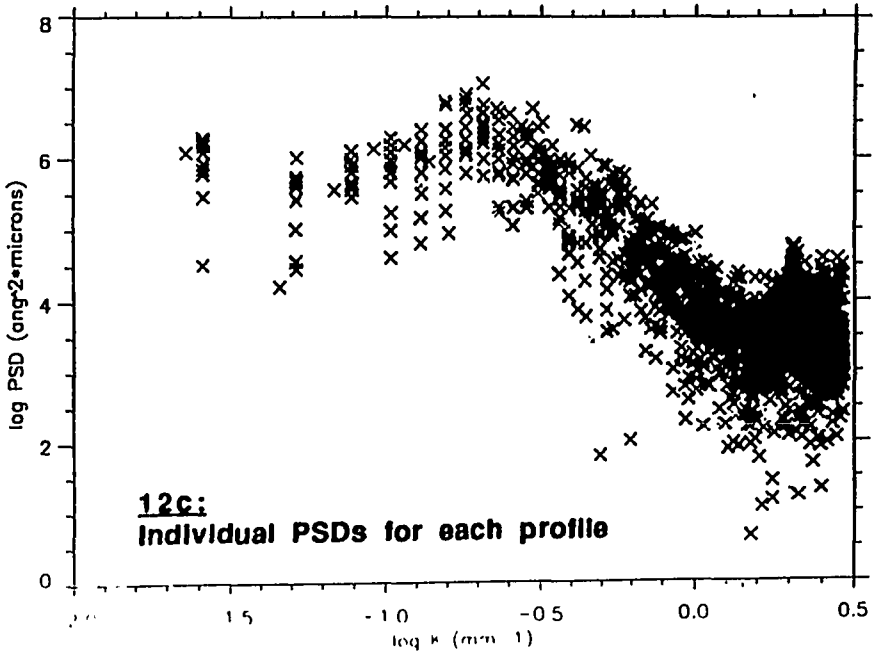

12c:
Individual PSDs for each profile

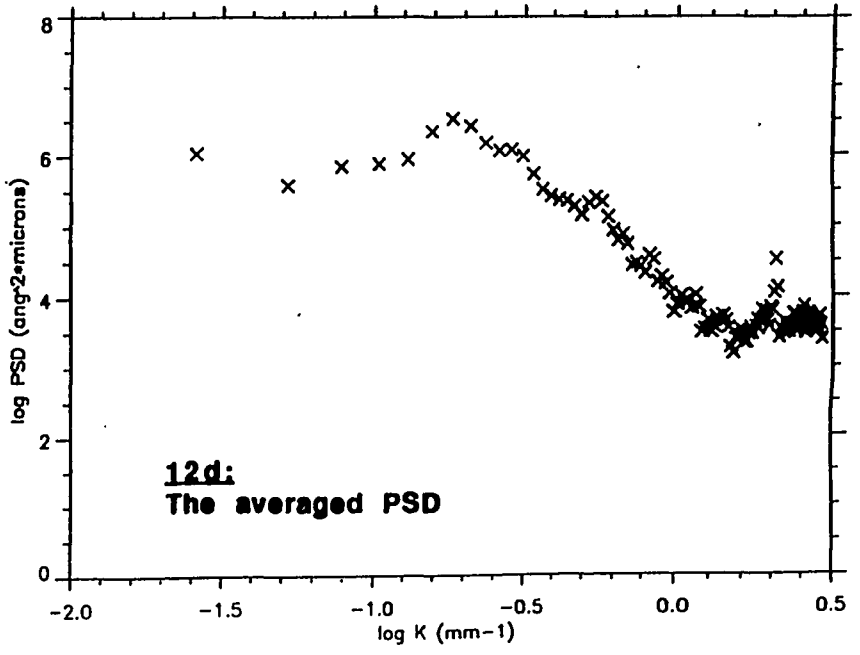

12d:
The averaged PSD

Figure 12:
Example of 1-D Fourier analysis of a transmitted wavefront

13a:
Phase map data

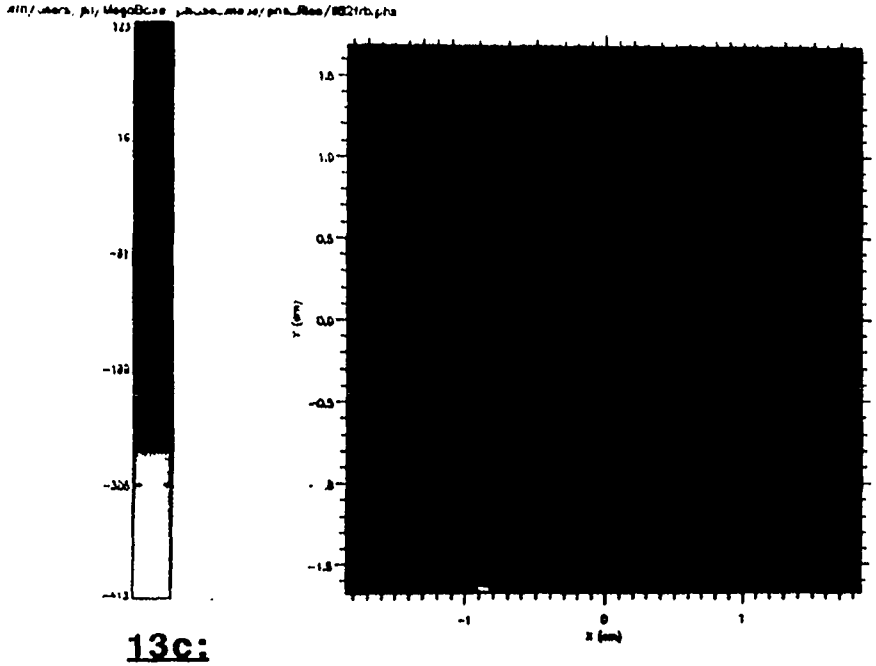

13b:
Phase map with Hanning window applied

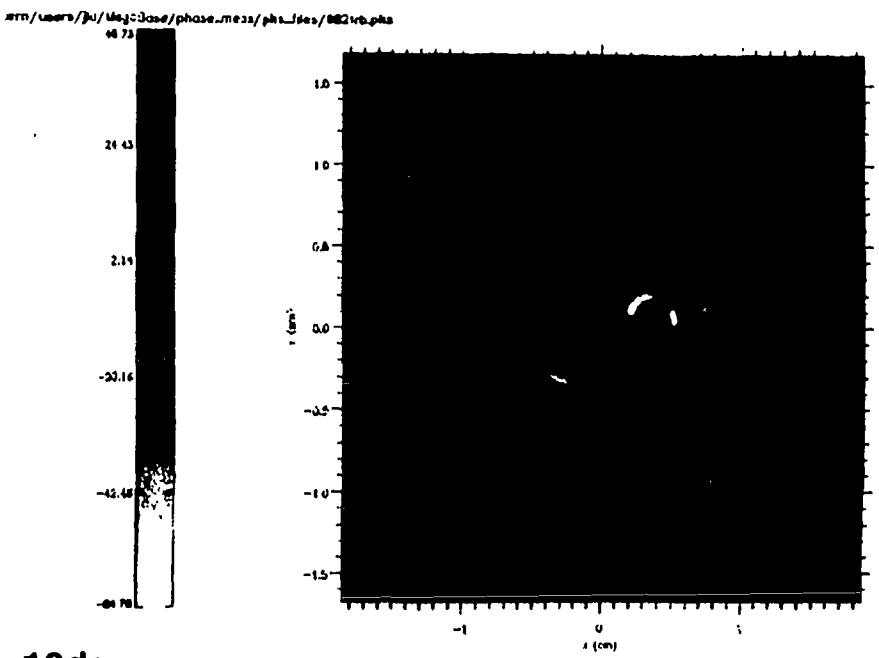

13c:
PSD calculated in 2-D

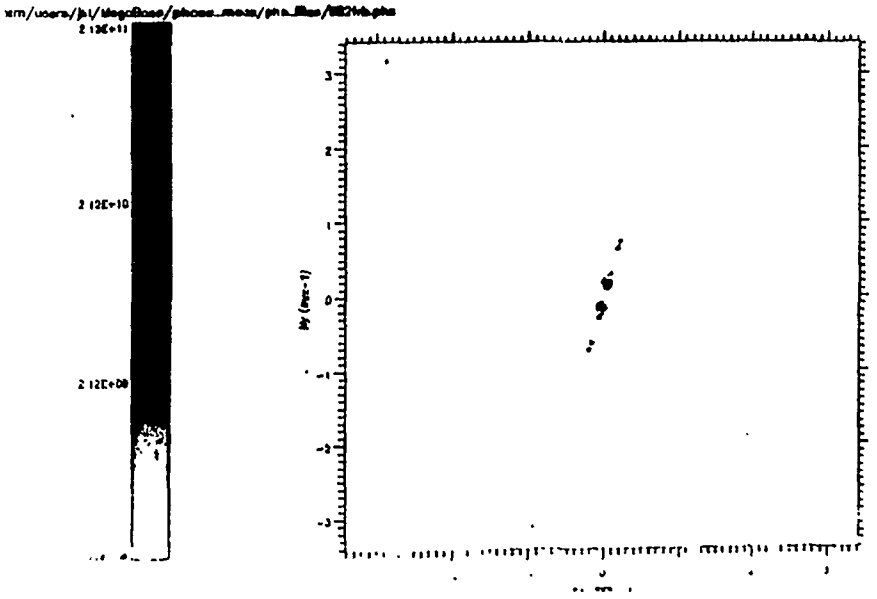

13d:
PSD surface

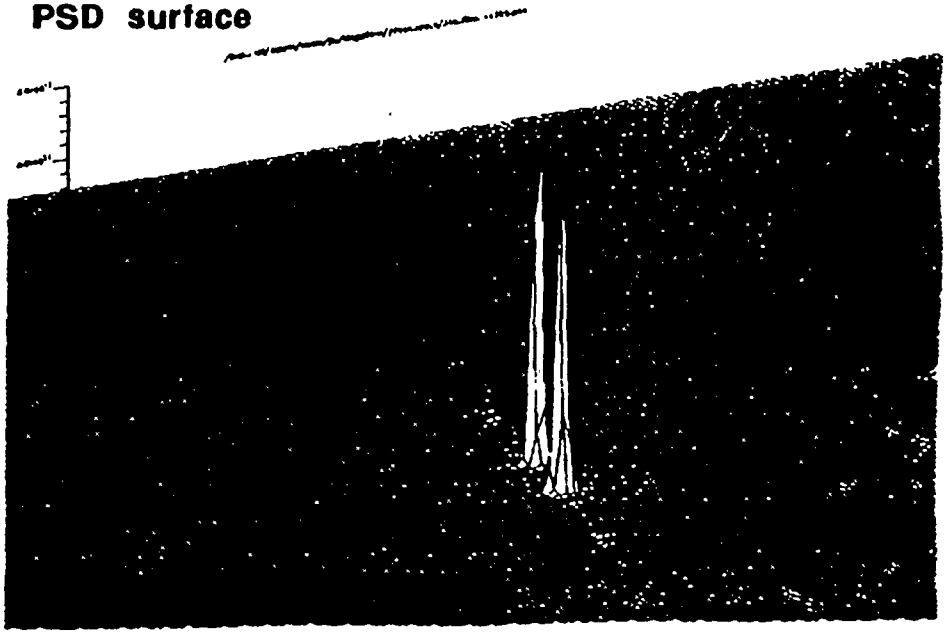

Figure 13:
Examples of 2-D Fourier analysis of a reflected wavefront (same data as Fig. 11)

14a:
Phase map data

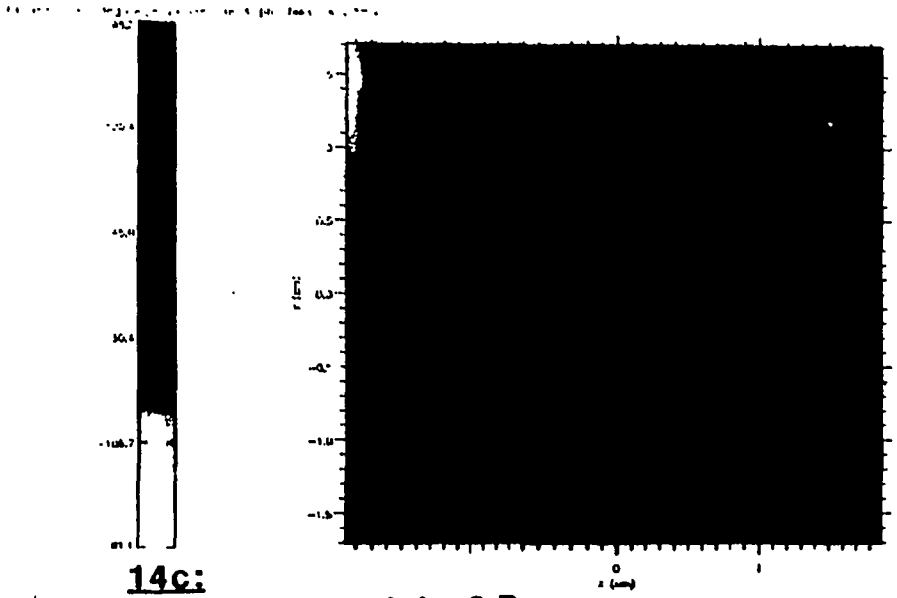

14b:
Phase map with Hanning window applied

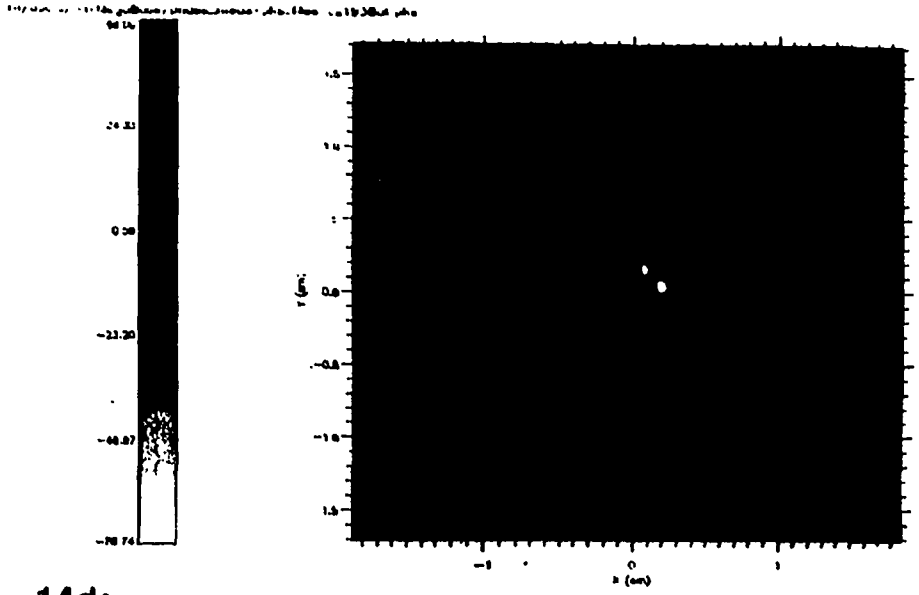

14c:
PSD calculated in 2-D

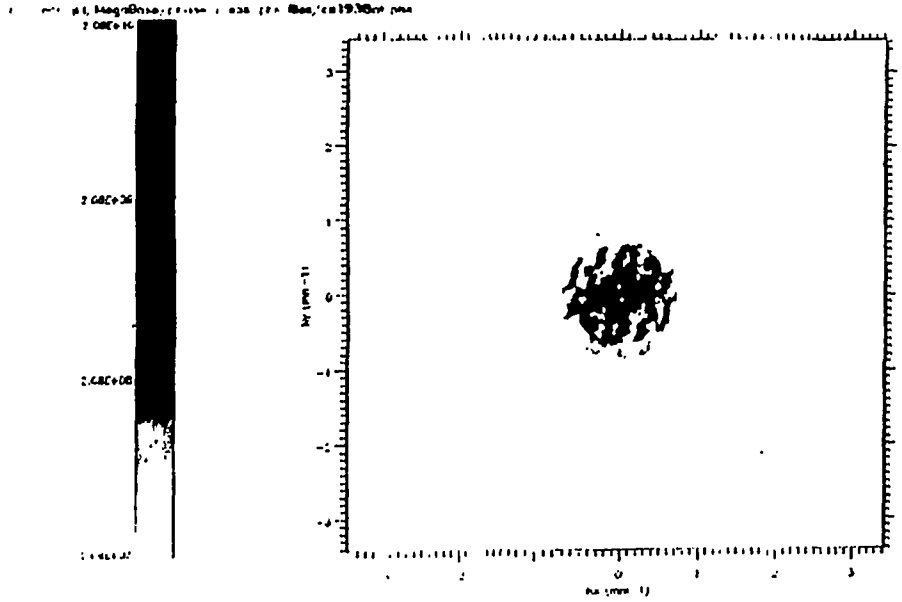

14d:
PSD surface

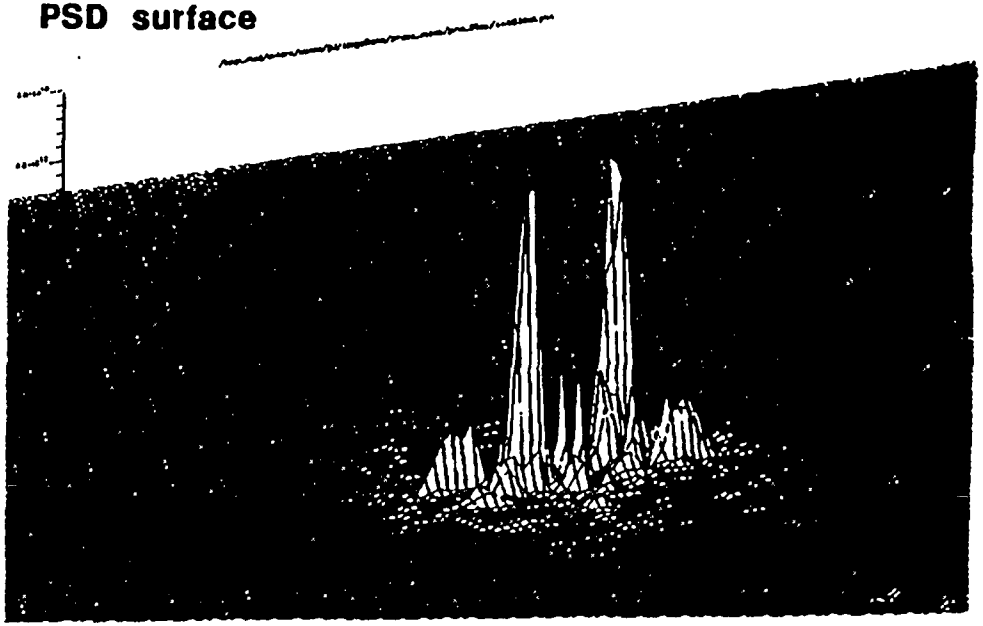

Figure 14:
Examples of 2-D Fourier analysis of a transmitted wavefront (same data file as Figure 12)